PAPER

Dielectric tuned circular dichroism of L-shaped plasmonic metasurface

IOP Publishing Journal of Physics D: Applied Physics
J. Phys. D: Appl. Phys. **50** (2017) 504001 (7pp) https://doi.org/10.1088/1361-6463/aa95f6

Dielectric tuned circular dichroism of L-shaped plasmonic metasurface

Yu Qu[1], Zhidong Zhang[2], Tong Fu[1], Gang Wang[1], Tiankun Wang[1], Mingyan Wang[1], Yu Bai[1] and Zhongyue Zhang[1]

[1] School of Physics and Information Technology, Shaanxi Normal University, Xi'an 710062, People's Republic of China
[2] Science and Technology on Electronic Test & Measurement Laboratory, North University of China, Taiyuan 030051, People's Republic of China

E-mail: zyzhang@snnu.edu.cn

Received 30 June 2017, revised 13 October 2017
Accepted for publication 25 October 2017
Published 21 November 2017

Abstract

In this paper, a dielectric layer is introduced to tune circular dichroism (CD) of chiral plasmonic metasurfaces. The dielectric layer is used to control the optical phase of electric diploes in Born–Kuhn configurations. To prove our assumption, an L-shaped plasmonic metasurface consisting of two metallic slices is prepared by glancing angle deposition, and then an SiO_2 slice is deposited on one arm of the L-shaped metasurface. Experimental results reveal that CD of the L-shaped plasmonic metasurface can be tuned by the thickness of the SiO_2 slice. These findings not only contribute to a better understanding of the CD physical mechanism, but also can be used in nanophotonic metasurfaces because of the concise fabrication process.

Keywords: circular dichroism, glancing angle deposition, chirality, plasmonics

(Some figures may appear in colour only in the online journal)

Introduction

Circular dichroism (CD) originated from the different absorption coefficients for left circularly polarized (LCP) and right circularly polarized (RCP) light in chiral structures. Most naturally chiroptical effects are inherently faint because the dipole moments of the chiral molecules occur over a markedly smaller distance than the helical pitch of circularly polarized light [1, 2]. Meanwhile, artificial chiral plasmonic nanostructures (CPNs) can solve this problem by enhancing the chiral response by light matter interactions [3–6]. Recently, the chiroptical effects of CPNs gathered considerable attention because of their advantageous applications, such as circular polarization [7, 8], negative refraction [9], and bio-sensing [10].

CD may arise from different mechanisms. Previous studies have shown that CD of CPNs stems from the electric or magnetic dipole mode [6, 11]. In general, certain CPNs can produce both electrical and magnetic responses, and CD originates from the coupling interaction when magnetic dipole is not perpendicular to electric dipole of CPNs. To generate

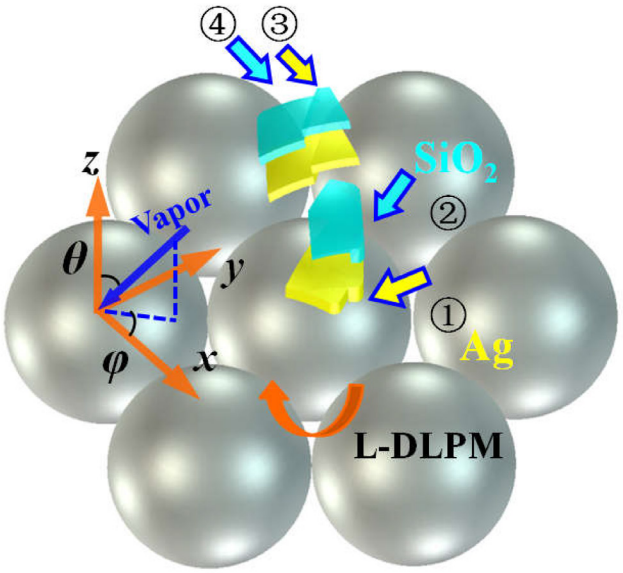

Figure 1. Schematics of deposition process for DLPM on PS nanosphere included four steps. The direction of each deposition is indicated by the arrows marked numbers.

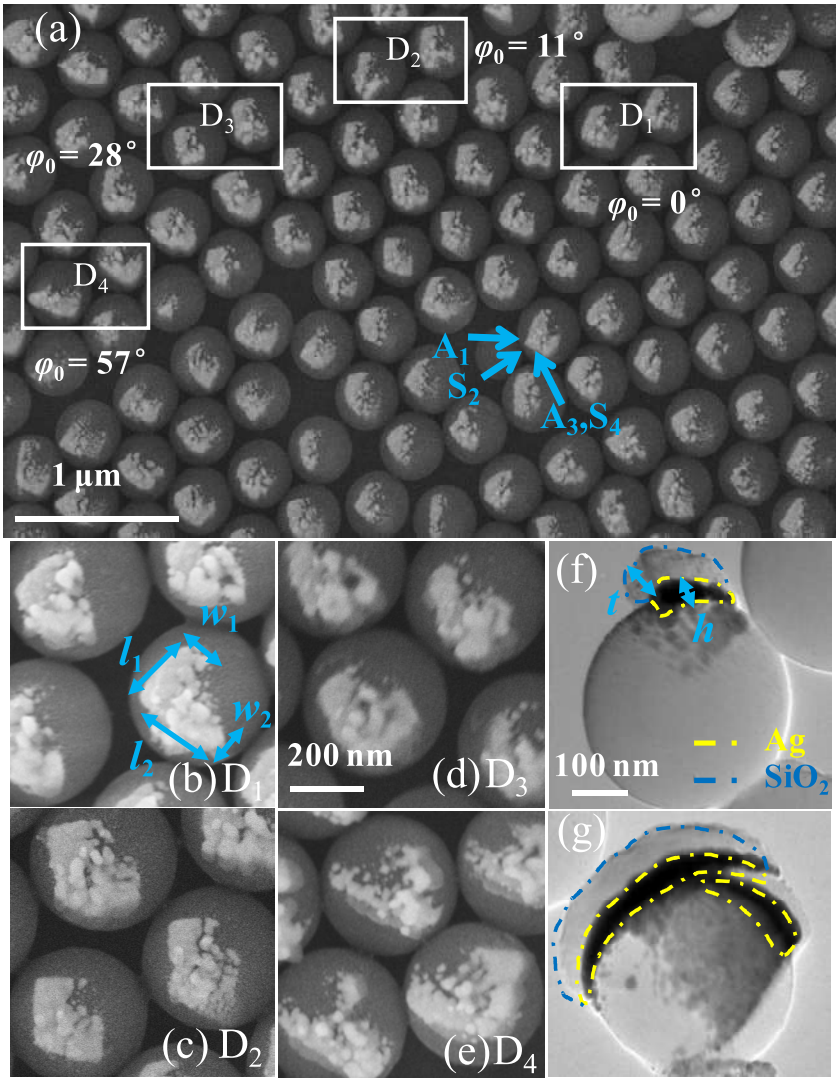

Figure 2. (a)–(e) Top-view SEM images of the L-DLPM on $d = 380$ nm nanosphere monolayers, the directions of depositions are shown by blue arrows marked as A_1, S_2, A_3, S_4. (f) and (g) TEM images of the L-DLPM cross-sections. Yellow and blue dashed lines are Ag slices and SiO_2 slice, respectively.

the coupling interaction, several researchers have considered oblique incidence to excite the extrinsic chirality of nanostructures regardless of whether these nanostructures are chiral or not [12–14]. When parallel nanorice heterodimers are illuminated at oblique angles, the coupling of the electric dipole and magnetic dipole of two nanorices results in CD [14]. In addition, several researchers indicated that the magnetic and electric responses of CPNs can be switched by changing the polarization of incident light or thickness of structure [15, 24]. The different electric diploes coupling can also achieve CD. Ag nanohelixes are proposed to produce different collective charge oscillations along the helix. CD is attributed to the coupling between electric dipoles of adjacent pitches and can be tuned by the half-pitch of helix [7, 16–20]. According to recent studies, CD can be interpreted by two cross electric diploes in bi-layer CPNs, specifically, the bonding and antibonding modes of Born–Kuhn (B–K) configuration. Under LCP and RCP light, the twist charge oscillation modes produce a phase retardation effect, which leads to CD [21–25].

In this paper, a dielectric layer is introduced to control the optical phase of electric diploes in B–K model. To realize this assumption, we designed L-shaped plasmonic metasurface (LPM) composed by two separate Ag slices, and used a dielectric SiO_2 slice to cover in one arm of the L-shaped plasmonic metasurface (DLPM) to tune CD. The designed metasurface is fabricated on self-assembled PS sphere templates by using glancing angle deposition (GLAD) in experiment. GLAD is regarded as an industrial technique to fabricate the CPNs because of its low cost and scalability; its mechanism is the geometric shadowing effect [18, 20, 24–26]. Experimental results show that the DLPM exhibits a strong CD than that of LPM without the SiO_2 slice. By increasing the thickness of SiO_2 slice, the optical phase variation of cross-electric dipoles on the two metallic slices increases, resulting in increasing CD. These findings not only contribute to a better understanding of the CD physical mechanism but also can be used in preparing nanophotonic metasurfaces because of the concise fabrication process.

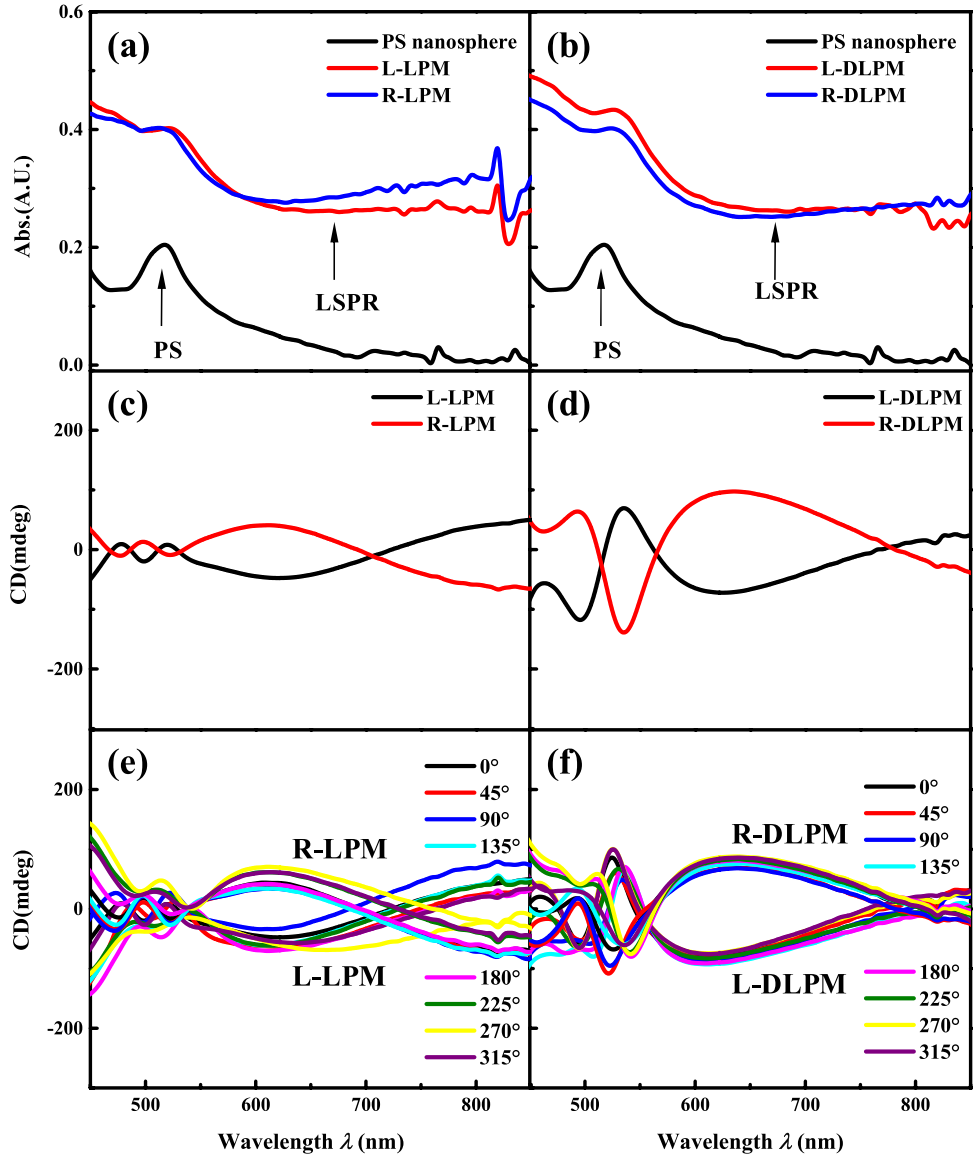

Figure 3. (a) and (b) The absorption spectra of the LPM and DLPM under the unpolarized light illumination. (c) and (d) The CD spectra of the LPM and DLPM. (e) and (f) The rotation measure of CD spectra of the LPM and DLPM.

Results and discussion

The fabrication of the DLPM starts with the self-assembled polystyrene (PS) nanosphere (diameter $d = 380\,\text{nm}$) monolayers on glass substrates with size of $1.1\,\text{cm} \times 2.4\,\text{cm}$. More details on the preparation of the PS nanosphere can be found in our previous work in [24, 25]. Four steps of deposition are needed to fabricate the DLPM through GLAD. Both depositions adopted the same tilt angle of $\theta = 86°$ with respect to the normal substrate, as shown in figure 1. Here, φ is defined as the angle of the substrate azimuthal orientation. In the first step, Ag vapors are deposited onto monolayers with $\varphi = 0°$. In the second step, the substrate is rotated clockwise at an angle of $\varphi = 30°$ for the deposition of SiO_2 vapors. In the third step, the substrate is rotated clockwise at an angle of $\varphi = 120°$ to deposit Ag vapors, and then the L-shaped nanoslices is achieved. In the fourth step, SiO_2 vapors are deposited on one arm of the L-shaped nanoslices with $\varphi = 120°$. The second deposition is used to separate the two arms of the L-shaped nanoslices. The thicknesses of different layers are controlled by the deposition time of the E-beam evaporator. This deposition can form the left-helical DLPM (L-DLPM), and for the right-helical DLPM (R-DLPM), the substrate is rotated anticlockwise at angles of $\varphi = -30°$ and $-120°$ in the second and third steps.

Figure 2(a) shows a representative top-view scanning electron microscopy (SEM) image of the L-DLPM. The period of the DLPM obtained by the above process is hexagonal. The L-DLPM possessed a distinct morphology in the large-scale area because of the different orientations of the template of hexagonal close-packed PS nanospheres. Four distinct domains are marked as D_1, D_2, D_3, and D_4. To illustrate the mechanism for forming different domains, we define each domain by using the azimuthal angle φ_0 with respect to the first Ag deposition φ. The initial φ can be degenerated as $\varphi = \varphi_0 + n \cdot 60°$ because of the symmetry of the hexagonal close-packed lattice for $0° \leqslant \varphi_0 < 60°$, where n is an integer. As shown in figure 2(a), $\varphi_0 = 0°$, 11°, 28°, 57°. In simulation, we choose

one domain with an orientation of 11°. The blue arrows denote the first deposition Ag (marked as A_1), second deposition SiO_2 (marked as S_2), third deposition Ag (marked as A_3), and fourth deposition SiO_2 (marked as S_4). Due to the random direction of the hexagonal close-packed PS nanospheres, SiO_2 is deposited either on the long arm of L-shaped nanostructure or on the short arm. The relevant higher-magnification SEM images are shown in figures 2(b)–(e). To measure the actual length and width values of the L-DLPM, we performed a statistical study on the domain distribution of side length. As illustrated in figure 2(b), the measured length and width values of the L-DLPM are $l_1 = 200\,\text{nm}$, $l_2 = 210\,\text{nm}$, $w_1 = 110\,\text{nm}$, and $w_2 = 100\,\text{nm}$, respectively. Figures 2(f) and (g) shows the transmission electron microscopy (TEM) of the cross-sections of the L-DLPM. Ag slices and SiO_2 slice are presented by the yellow and blue dashed lines, respectively. The two Ag slices are separated by the SiO_2 gap. The actual thickness of each Ag or SiO_2 slice is estimated to be about $h = 30\,\text{nm}$ and $t = 40\,\text{nm}$, which proportionately decreased due to oblique incident of vapor source, varying from the deposited thickness ($H = 50\,\text{nm}$ and $T = 50\,\text{nm}$) set in the E-beam evaporator. In this paper, the thickness of fourth SiO_2 slice is varied to tune the CD of the DLPM.

The CD spectra were measured with normal incidence of light from $\lambda = 450\,\text{nm}$ to 850 nm by Chirascan (Applied Photophysics Ltd.). The absorbance signals difference CD is given by $\theta\,(\text{mdeg}) = 33\,000 * \Delta A$, where ΔA is the absorbance difference of LCP and RCP irradiations. Figures 3(a) and (b) depict the unpolarized absorption of the PS nanosphere, the LPM, and the DLPM with the thicknesses of Ag and SiO_2 fixed at $H = 50\,\text{nm}$ and $T = 50\,\text{nm}$, respectively. The black line marked as 'PS' represents the absorption peak of the PS nanosphere, which is the first diffracted order of manolayer nanosphere arrays [25]. A broad peak appears at $\lambda = 650\,\text{nm}$, and this peak corresponds to the localized surface plasmon resonance (LSPR) of the Ag layer. The unpolarized absorption of the LPM and the DLPM showed no distinct handedness-dependent feature. The CD spectra of the LPM and the DLPM are shown in figures 3(c) and (d). For the L-DLPM, the spectrum shows negative CD signals at around $\lambda = 635\,\text{nm}$ and $\lambda = 495\,\text{nm}$, meaning that the absorption of LCP light is less than that of RCP light. The positive CD signals occur at around $\lambda = 535\,\text{nm}$ due to the stronger excitation efficiency of LCP light than that of RCP light. Here only the two modes of $\lambda = 635\,\text{nm}$ and $\lambda = 535\,\text{nm}$ are considered because of the first diffracted order at $\lambda = 515\,\text{nm}$. The CD spectra for the L-DLPM and R-DLPM are in mirrored symmetry to each other. Due to the anisotropy morphology of the individual DLPM, linear dichroism (LD) and birefringence may not be negligible. We measured the CD spectra of the LPM and the DLPM at different azimuthal orientations with respect to the substrate. As shown in figures 3(e) and (f), the rotation measurement spectra show robust CD signals with varied azimuthal orientations of sample, which reveal the linear anisotropy effects are ignorable in CD spectra; namely, the CD mainly come from chirality of the L-shaped Ag slices.

To study how the SiO_2 thickness influences the CD signals of the DLPM, we presented the CD spectra with increasing T in figure 4(a). With the increase in thickness T from 0 nm to 75 nm, the values of CD modes at around $\lambda = 635\,\text{nm}$ (marked as I) and $\lambda = 535\,\text{nm}$ (marked as II) of the L-DLPM are both enhanced and red shifted. The same trends of enlargement and red shift also occurred in the R-DLPM with increasing T. In addition, the dissymmetry factor g, a dimensionless quantity factor, is a parameter to evaluate the chirality of a chiral structure. The g factor of the DLPM is calculated as shown in figure 4(b). The g factor is defined as $g = \Delta A/A$, where $\Delta A = \text{CD (mdeg)}/33\,000$ is the differential absorption between LCP and RCP light and A is the unpolarized absorption. The g factor characteristics of enlargement and red shift with increasing T are similar with that of the CD spectra. The magnitude of the g factor can reach 0.02 at the peak of $\lambda = 535\,\text{nm}$ for the L-DLPM.

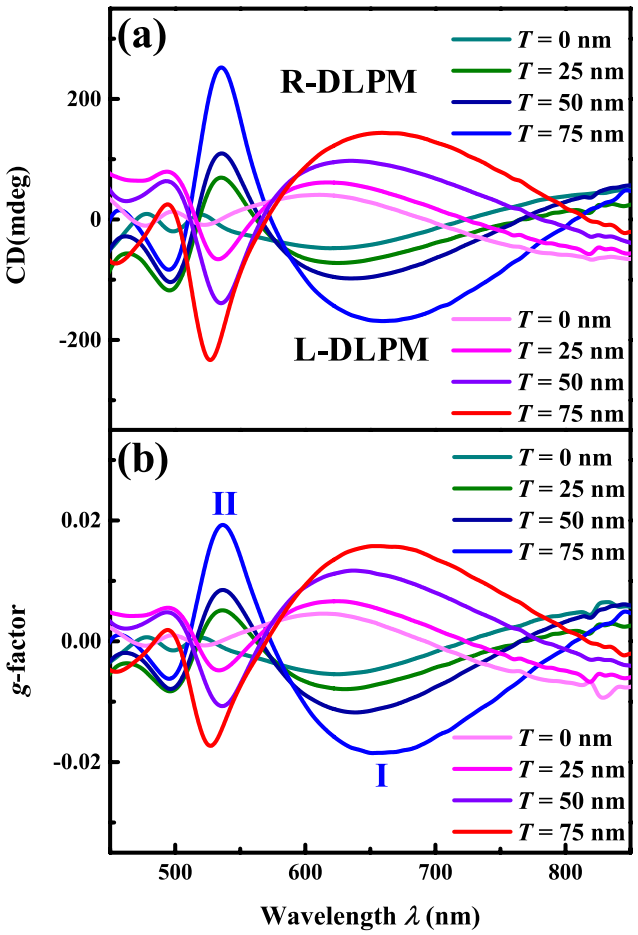

Figure 4. The CD and g factor spectra of and DLPM with varied thicknesses of SiO_2 slice.

To explore the mechanism of the tunable CD, the absorption of the L-DLPM arrays is numerically simulated by the finite element method (COMSOL Multiphysics). Figure 5(a) illustrates the simplified geometric models of the L-DLPM arrays, in which the height difference between two slices is ignored. The refractive index of air and SiO_2 is regarded as 1 and 1.45, respectively. The frequency dependent permittivity of silver is taken from the [27], modified to include the size effect. The excitation sources are RCP and LCP light along the $-z$ direction and the magnitude of the incident electric field is set at 1 V m^{-1}. The infinite array simulated using periodic boundary

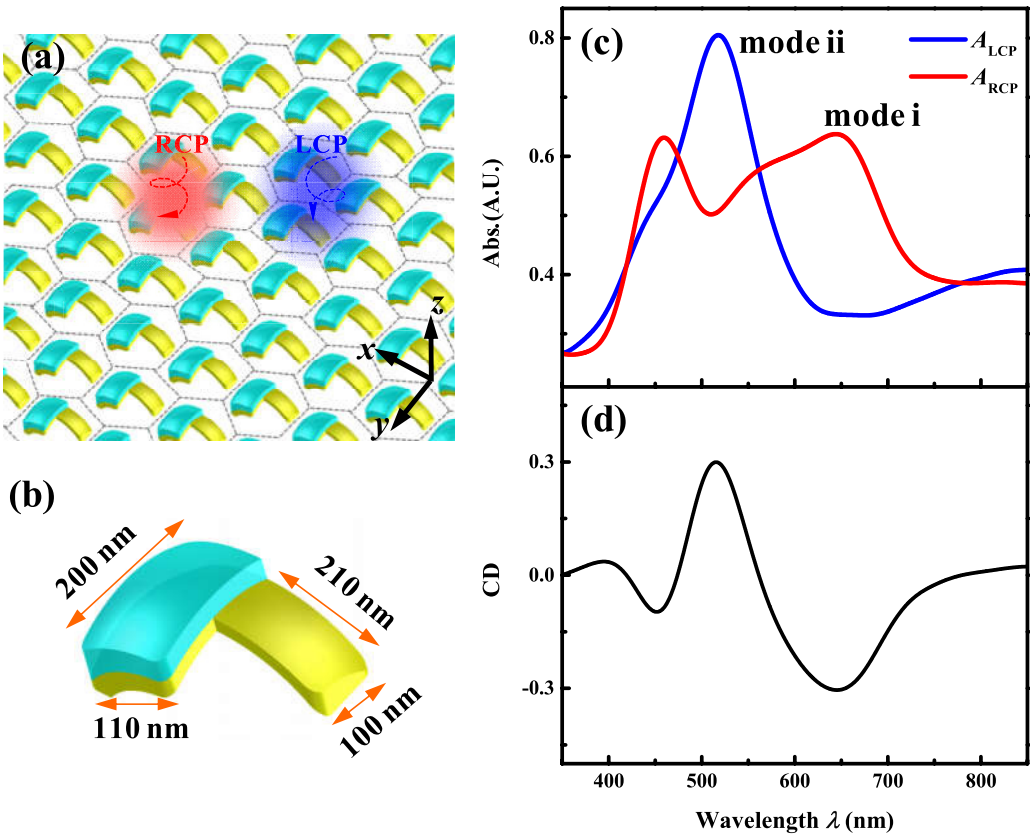

Figure 5. (a) and (b) The geometric model arrays and the parameters definition of the L-DLPM. (c) and (d) The simulated absorbance and CD spectra of the L-DLPM arrays.

conditions along the hexagonal unit cell. The CD effect was defined as $CD = A_{LCP} - A_{RCP}$, where A_{RCP} and A_{LCP} is the absorbance under RCP and LCP illumination. The unit cell with the associated parameters set according to the SEM and TEM data is displayed in figure 5(b). The thickness of each Ag slice and SiO_2 slice is $h = 30$ nm and $t = 40$ nm, respectively. The lengths and widths of one Ag arm are defined as 200 nm and 110 nm, whereas those of the other arm are 210 nm and 100 nm, respectively. The lengths and widths of the SiO_2 layer are fixed at 200 nm and 110 nm. The angle between two arms is 90°. The absorbance and CD spectra of the L-DLPM are shown in figures 5(c) and (d) under LCP and RCP irradiations. The two resonant modes at around $\lambda = 650$ nm and 510 nm are marked as mode i and mode ii in absorbance spectra. The different intensities of absorbance at the resonant wavelength result in distinct CD signals. However, due to the average effect in the size and shape of the L-DLPM obtained experimentally, the position and resonant intensity of CD spectrum present certain deviations compared with the experimental results.

For investigating the CD mechanism, the characters of the L-DLPM under LCP and RCP illumination have been analyzed. The near-field charge density distributions are examined at resonant wavelengths, as depicted in figure 6. For convenient analysis of the modes, the equivalent electric dipole moments are marked by black arrows and labeled as 'P_a' and 'P_b'. In mode i at $\lambda = 650$ nm for the LCP light, the effective charge oscillation on one slice forms the equivalent electric dipole P_a along the diagonal of slice, and electric dipole P_b of the other slice is along the short axis of slice. The strong near-field

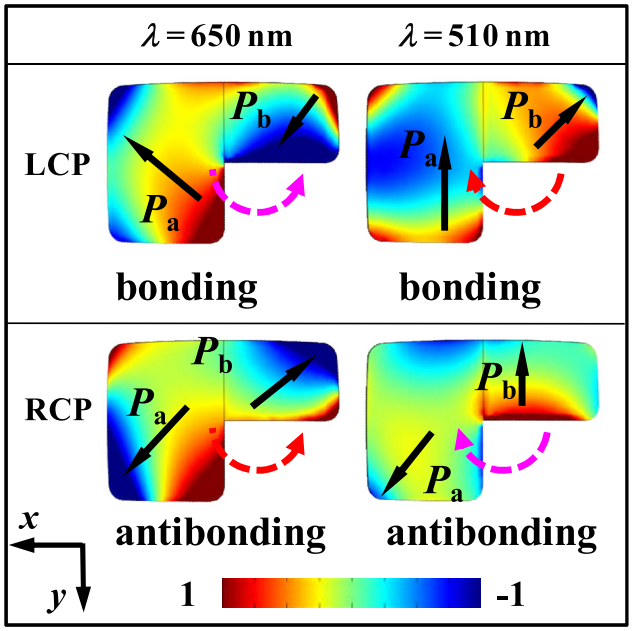

Figure 6. The resonant modes expressed by the charge density distribution on L-shaped Ag arms at resonant wavelengths. Red is positive charge whereas blue is negative charge. The black arrows represent the equivalent electric dipole moments.

coupling of the two cross electric dipoles forms the bonding mode (B–K model), the vector of which is at an angle [22]. The two electric dipoles can be taken as antibonding mode for the RCP light. The P_a needs to rotate clockwise to parallel

to the P_b, as shown by the pink dotted arrow, which exerts a negative effect on LCP [28]. While for RCP light the P_a also needs to rotate clockwise to parallel to the P_b (marked as the red dotted arrow), and shows positive effect on RCP. This different effect results in the negative CD dip. Similarly, at mode ii, the bonding mode has positive effect on LCP whereas the antibonding mode has negative effect on RCP, which produces the positive CD peak. Due to the introduction of the dielectric SiO_2 slice upon one arm of the nanoslices, the optical phase of the P_b is larger than the P_a. As the thickness of dielectric SiO_2 slice increases, the phase retardation effects of the two cross electric dipoles become more evident, and CD is enhanced.

Conclusion

In summary, a method for controlling the phase difference of Born–Kuhn model to generate tunable CD is proposed. Experimental results show that the designed L-shaped plasmonic metasurface can produce enhanced CD with the increasing thickness of the dielectric SiO_2 slice. Under LCP and RCP illuminations, the two cross electric dipoles in two Ag arms provide a phase difference owing to the varied dielectric environment of SiO_2 slice, which results in the CD signals. This study not only provides a concise and scalable method for fabricating chiral plasmonic metasurfaces but also contributes to the understanding of the CD generation mechanism.

Acknowledgments

This work was partially funded by the National Natural Foundation of China (Grant Nos. 61575117 and 61605177), the Fundamental Research Funds for the Central Universities of Ministry of Education of China (Grant No. GK201601008), the Fundamental Research Funds for the Central Universities (2017TS012) and the Fundamental Research Funds for the Central Universities (2016TS037).

ORCID iDs

Zhongyue Zhang https://orcid.org/0000-0002-2834-429X

References

[1] Takezaki M and Kito Y 1967 Circular dichroism of rhodopsin and isorhodopsin *Nature* **215** 1197–9
[2] Barron L D 2004 *Molecular Light Scattering and Optical Activity* (Cambridge: Cambridge University Press)
[3] Valev V K, Baumberg J J, Sibilia C and Verbiest T 2013 Chirality and chiroptical effects in plasmonic nanostructures: fundamentals, recent progress, and outlook *Adv. Mater.* **25** 2517–34
[4] Tang Y and Cohen A E 2010 Optical chirality and its interaction with matter *Phys. Rev. Lett.* **104** 163901
[5] Schäferling M, Dregely D, Hentschel M and Giessen H 2012 Tailoring enhanced optical chirality: design principles for chiral plasmonic nanostructures *Phys. Rev.* X **2** 031010
[6] Eftekhari F and Davis T J 2012 Strong chiral optical response from planar arrays of subwavelength metallic structures supporting surface plasmon resonances *Phys. Rev.* B **86** 075428
[7] Gansel J K, Thiel M, Rill M S, Decker M, Bade K, Saile V and Wegener M 2009 Gold helix photonic metamaterial as broadband circular polarizer *Science* **325** 1513–5
[8] Yu Y, Yang Z, Li S and Zhao M 2011 Higher extinction ratio circular polarizers with hetero-structured double helical metamaterials *Opt. Express* **19** 10886–94
[9] Zhou J, Dong J, Wang B, Koschny T, Kafesaki M and Soukoulis C M 2009 Negative refractive index due to chirality *Phys. Rev.* B **79** 121104
[10] Hendry E, Carpy T, Johnston J, Popland M, Mikhaylovskiy R V, Lapthorn A J and Kadodwala M 2010 Ultrasensitive detection and characterization of biomolecules using superchiral fields *Nat. Nanotechnol.* **5** 783–7
[11] Kuwata-Gonokami M, Saito N, Ino Y, Kauranen M, Jefimovs K, Vallius T, Turunen J and Svirko Y 2005 Giant optical activity in quasi-two-dimensional planar nanostructures *Phys. Rev. Lett.* **95** 227401
[12] Papakostas A, Potts A, Bagnall D M, Prosvirnin S L, Coles H J and Zheludev N I 2003 Optical manifestations of planar chirality *Phys. Rev. Lett.* **90** 107404
[13] Lu X X, Wu J, Zhu Q N, Zhao J W, Wang Q B, Zhan L and Ni W H 2014 Circular dichroism from single plasmonic nanostructures with extrinsic chirality *Nanoscale* **6** 14244–53
[14] Tian X R, Fang Y R and Zhang B 2014 Multipolar Fano resonances and Fano-assisted optical activity in silver nanorice heterodimers *ACS Photon.* **1** 1156–64
[15] Xiong X, Sun W H, Bao Y J, Peng R W, Wang M, Sun C, Lu X, Shao J, Li Z F and Ming N B 2009 Switching the electric and magnetic responses in a metamaterial *Phys. Rev.* B **80** 201105
[16] Kuzyk A, Schreiber R, Fan Z, Pardatscher G, Roller E M, Högele A, Simmel F C, Govorov A O and Liedl T 2012 DNA-based self-assembly of chiral plasmonic nanostructures with tailored optical response *Nature* **483** 311–4
[17] Hentschel M, Wu L, Schäferling M, Bai P, Li E P and Giessen H 2012 Optical properties of chiral three-dimensional plasmonic oligomers at the onset of charge-transfer plasmons *ACS Nano* **6** 10355–65
[18] Song C, Blaber M G, Zhao G, Zhang P, Fry H C, Schatz G C and Rosi N L 2013 Tailorable plasmonic circular dichroism properties of helical nanoparticle superstructures *Nano Lett.* **13** 3256–61
[19] He Y, Larsen G K, Ingram W and Zhao Y P 2014 Tunable three-dimensional helically stacked plasmonic layers on nanosphere monolayers *Nano Lett.* **14** 1976–81
[20] Mark A G, Gibbs J G, Lee T C and Fischer P 2013 Hybrid nanocolloids with programmed three-dimensional shape and material composition *Nat. Mater.* **12** 802–7
[21] Decker M, Ruther M, Kriegler C E, Zhou J, Soukoulis C M and Wegener M 2009 Strong optical activity from twisted-cross photonic metamaterials *Opt. Lett.* **34** 2501–3
[22] Yin X H, Schäferling M, Metzger B and Giessen H 2013 Interpreting chiral nanophotonic spectra: the plasmonic Born–Kuhn model *Nano Lett.* **13** 6238–43
[23] Qu Y, Huang L S, Wang L and Zhang Z Y 2017 Giant circular dichroism induced by tunable resonance in twisted Z-shaped nanostructure *Opt. Express* **25** 5480–7
[24] Fu T, Qu Y, Wang T, Wang G, Wang Y, Li H, Li J, Wang L and Zhang Z Y 2017 Tunable chiroptical response of chiral plasmonic nanostructures fabricated with chiral templates

through oblique angle deposition *J. Phys. Chem.* C **121** 1299–304
[25] Wang Y, Deng J, Wang G, Fu T, Qu Y and Zhang Z Y 2016 Plasmonic chirality of L-shaped nanostructure composed of two slices with different thicknes *Opt. Express* **24** 2307–17
[26] Larsen G K, He Y, Ingram W, LaPaquette E T, Wang J and Zhao Y P 2014 The fabrication of three-dimensional plasmonic chiral structures by dynamic shadowing growth *Nanoscale* **6** 9467–76
[27] Johnson P B and Christy R W 1972 Optical constants of the noble metals *Phys. Rev.* B **6** 4370–9
[28] Wang T K, Fu T, Chen Y Y and Zhang Z Y 2017 Circular dichroism of a tilted U-shaped nanostructure *Opt. Lett.* **42** 2842–5